ENHANCED KINEMATIC POSITIONING METHODS BY SHAPING FILTER AUGMENTATION

Katrin Ramm
Institute for Applications of Geodesy to Engineering
Universität Stuttgart
Email: katrin.ramm@iagb.uni.stuttgart.de

Abstract: Kalman filtering is an important tool for positioning for vehicle navigation and for location based services. This paper, therefore, deals with methods to enhance a standard Kalman filter approach for kinematic positioning. Any modelling of Kalman filter approaches requires white measurement and process noise. GPS positions as input quantities do not meet these requirements due to existence of autocorrelation. Red noise has to be assumed due to slowly changing measurement deviations caused by tropospheric propagation delay, for example. In a first step, the filter respectively the state vector is augmented by a shaping filter to consider red noise of kinematic GPS positions. The appropriate autocorrelation function is a bell-shaped curve and its characteristic parameter - the attenuation factor - is determined empirically. So data of some test runs (approx. 650 km, driven with the measuring vehicle of the institute (MOdular Positioning SYstem (MOPSY), see [21])) are evaluated by time series analysis. The resulting autocorrelation functions are approximated by regression analysis to derive a functional description. In a next step, the attenuation factor is supposed to be unknown because of uncertainties in determining it accurately. Therefore a second approach is proposed to estimate the attenuation factor by an adaptive estimation for the augmented Kalman filter. These approaches are evaluated with respect to the standard one. Both simulated data to conduct variance-based sensitivity analysis and real data are used.

1. Motivation

One research focus of the institute for applications of geodesy to engineering (IAGB) is modelling of vehicle motion by Kalman filtering. Several modifications for improvements of position estimation are developed. This paper focuses on correct stochastic modelling especially of the DGPS kinematic measurements. Improvements are expected for the quality of the different filter tests, significantly influencing the filter performance, and for more realistic accuracy estimations. Sensitivity analysis enables the investigations of dependencies between output and input uncertainties, thus giving hints for further improvements.

2. Kinematic DGPS Data Analyses

Various investigations in literature deal with the improvement of stochastic modelling for GPS measurement evaluation. The focus is mainly set on GPS carrier phase measurements. Using a more realistic accuracy estimation it is expected to obtain more correct results in least squares adjustment.

The improvement of stochastic modelling can be achieved by taking autocorrelation into account due to coloured measurement noise. While mathematical correlations are often included in standard GPS software ([6], [7]), physical correlations are mostly neglected [8]. Physical correlations originate from incomplete modelling of slowly changing measurement deviations caused by tropospheric propagation delay and multipath ([9], [10]). They can result in time-related and/or spatial correlations [11].

Examinations regarding time-related correlations and their consideration in various evaluation models can be found in [7], [9], [11], for example. The data analyses presented in this chapter aim to determine the specific autocorrelation function for positions generated from differential kinematic code measurements.

	test run 1	**test run 2**	**test run 3**	**test run 4**
characteristics	country roads, motorways	motorways	country roads, hillside situation	rural area, small villages
epochs	12766	12601	8653	4348
duration in h	3:32	3:30	2:24	1:12
length in km	245.4	227.5	129.7	52.9
GPS available in %	94.0	96.3	97.3	90.9
GPS loss in %	6.0	3.7	2.7	9.1

Table 1: Statistic about the test runs

The data used are generated from four test runs in the vicinity of Stuttgart using MOPSY. The institute has taken these test runs within an industry project. Table 1 gives an overview about the statistics of the four test runs. As can be seen, data of approx. 650 km was taken. The availability of DGPS measurements differs due to different characteristics of the respective environments.

To determine the autocorrelation function time series analysis is carried out. Time-related correlations are preliminary caused by non or incompletely modelled errors. These correlations are supposed to be dependent of the direction of motion. Therefore the deviations of the DGPS positions to a Kalman filtered reference trajectory along and cross track are analysed. As a result, eight time series (four along and four cross track) have to be evaluated. After data pre-processing the autocovariance function of each time series is determined (see, e.g. [13]).

The empirically determined autocorrelation functions are approximated by a regression analysis to generate a functional model for consideration in the Kalman filter. Since the autocorrelation is high for small Δt and decreases fast, a red noise process is proposed. The appropriate approach for the model is a bell-shaped curve with attenuation factor β

$$\rho(\Delta t) = e^{-\beta^2 \Delta t^2} \tag{1}$$

The results of the time series analyses are summarised in table 2 and visualised in figure 1.

		reciprocal attenuation factor 1/beta in s
along track	test run 1	25.3
	test run 2	29.4
	test run 3	26.8
	test run 4	31.5
cross track	test run 1	29.1
	test run 2	30.1
	test run 3	29.5
	test run 4	34.3
average		**29.5**
stand. dev. (average)		**0.97**

Table 2: Estimation of the reciprocal attenuation factor $1/\beta$

The differences of the reciprocal attenuation factor between along and cross track are tested not to be significant. As a result, the overall average of $1/\beta = 30$ s is used further on both in modelling deviations along and cross track.

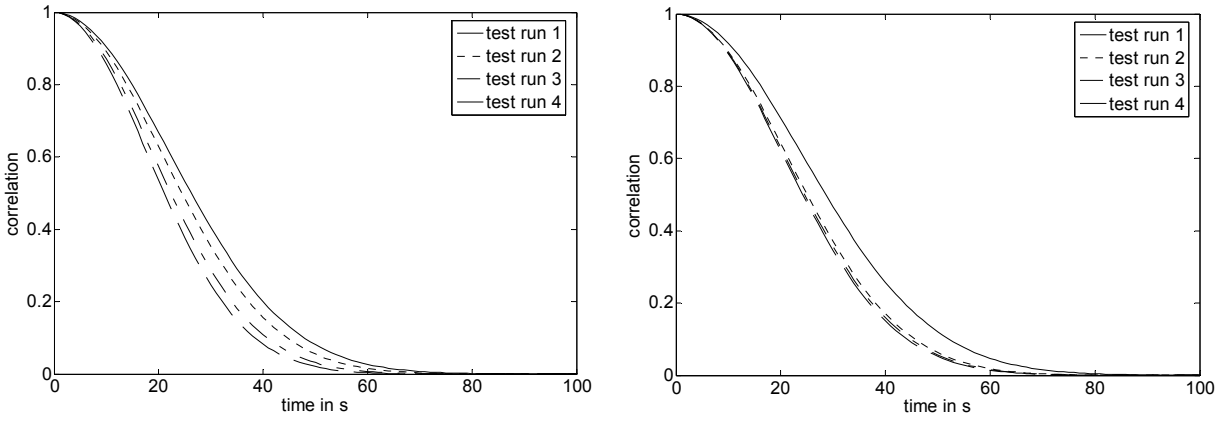

Figure 1: Autocorrelation functions approximated by regression analysis to a bell-shaped curve, along track (left) and cross track (right)

3. Kalman Filter Theory

This chapter provides a short introduction in shaping filter theory and additional adaptive filtering. The standard Kalman filter theory is omitted. For further information see [1] – [3].

3.1. Shaping Filter

As in standard Kalman filter, the shaping filter is divided into its two main parts. The system and the measurement equations:

$$\tilde{\boldsymbol{x}}_{k+1} = \boldsymbol{T}_{k+1,k} \cdot \tilde{\boldsymbol{x}}_k + \boldsymbol{B}_{k+1,k} \cdot \tilde{\boldsymbol{u}}_k + \boldsymbol{C}_{k+1,k} \cdot \boldsymbol{w}_k \tag{2}$$

$$\boldsymbol{l}_{k+1} = \boldsymbol{A}_{k+1} \cdot \tilde{\boldsymbol{x}}_{k+1} + \boldsymbol{\varepsilon}_{k+1} \tag{3}$$

Where equation (2) contains the model and provides the Kalman filter output given by the system state $\tilde{\boldsymbol{x}}_{k+1}$. Equation (3) delivers the functional relationship between the system state and the Kalman filter input, the measurements $\boldsymbol{l}_{k+1}$. In case of red measurement noise, instead

of $\boldsymbol{l}_{k+1}$ a measurement $\boldsymbol{l}'_{k+1}$ influenced by the noise $\boldsymbol{\varepsilon}^c_{k+1}$ including time-related correlation is given [4]. This can be expressed by the equation

$$\boldsymbol{l}'_{k+1} = \boldsymbol{l}_{k+1} + \boldsymbol{\varepsilon}^c_{k+1} \tag{4}$$

and leads to the following measurement equation

$$\boldsymbol{l}'_{k+1} = \boldsymbol{A}_{k+1} \cdot \widetilde{\boldsymbol{x}}'_{k+1} + \boldsymbol{\varepsilon}_{k+1}, \tag{5}$$

in which $\widetilde{\boldsymbol{x}}'_{k+1}$ is a systematically disturbed system state. To derive an undisturbed system state, the measurement equation has to be corrected

$$\boldsymbol{l}'_{k+1} = \boldsymbol{A}_{k+1} \cdot \widetilde{\boldsymbol{x}}_{k+1} + \boldsymbol{\varepsilon}_{k+1} + \boldsymbol{\varepsilon}^c_{k+1}, \tag{6}$$

in which $\boldsymbol{\varepsilon}_{k+1}$ is supposed to be white noise and $\boldsymbol{\varepsilon}^c_{k+1}$ red noise. Therefore the two noise parts can not be modelled by an increased measurement noise. Instead the red measurement noise has to be predicted using shaping filter augmentation ([2], [5]):

$$\boldsymbol{\varepsilon}^c_{k+1} = \boldsymbol{T}^c_{k+1,k} \cdot \boldsymbol{\varepsilon}^c_k + \boldsymbol{C}^c_{k+1,k} \cdot \boldsymbol{w}^c_k . \tag{7}$$

Within the transition matrix $\boldsymbol{T}^c_{k+1,k}$ the time-related behaviour of the red noise process is modelled and $\boldsymbol{w}^c_k$ is supposed to be white noise. The augmentation of the standard Kalman filter leads to the following system and measurement equations

$$\begin{vmatrix} \widetilde{\boldsymbol{x}}_{k+1} \\ \boldsymbol{\varepsilon}^c_{k+1} \end{vmatrix} = \begin{vmatrix} \boldsymbol{T}_{k+1,1} & \boldsymbol{0} \\ \boldsymbol{0} & \boldsymbol{T}^c_{k+1,k} \end{vmatrix} \cdot \begin{vmatrix} \widetilde{\boldsymbol{x}}_k \\ \boldsymbol{\varepsilon}^c_k \end{vmatrix} + \begin{vmatrix} \boldsymbol{B}_{k+1,1} \\ \boldsymbol{0} \end{vmatrix} \cdot \widetilde{\boldsymbol{u}}_k + \begin{vmatrix} \boldsymbol{C}_{k+1,k} & \boldsymbol{0} \\ \boldsymbol{0} & \boldsymbol{C}^c_{k+1,k} \end{vmatrix} \cdot \begin{vmatrix} \boldsymbol{w}_k \\ \boldsymbol{w}^c_k \end{vmatrix} \tag{8}$$

$$\boldsymbol{l}'_{k+1} = \begin{vmatrix} \boldsymbol{A}_{k+1} & \boldsymbol{A}^c_{k+1} \end{vmatrix} \cdot \begin{vmatrix} \widetilde{\boldsymbol{x}}_{k+1} \\ \boldsymbol{\varepsilon}^c_{k+1} \end{vmatrix} + \boldsymbol{\varepsilon}_{k+1} \tag{9}$$

This gives the main difference of the shaping filter to the standard Kalman filter. While the filter algorithm remains the same, by calculating the innovation the influence of the correlated fraction is removed from the prediction $\bar{\boldsymbol{x}}_{k+1}$

$$\boldsymbol{d}_{k+1} = \boldsymbol{l}'_{k+1} - \boldsymbol{A}_{k+1} \cdot \bar{\boldsymbol{x}}_{k+1} - \boldsymbol{A}^c_{k+1} \cdot \bar{\boldsymbol{\varepsilon}}^c_{k+1} . \tag{10}$$

The updated estimation of the system state is formulated with the predicted system state and the innovation, weighted by the gain matrix K (see e.g. [2]). Consequently, the updated system state is not falsified by the effects from red measurement noise.

3.2. Adaptive Shaping Filter

System equations may contain process coefficients. If these coefficients are only approximately known and are statistic quantities they can be determined together with the system state by adaptive filtering [3].

Within the adaptive shaping filter as it is understood here, uncertainties occurring in the shaping filter modelling should be taken into account. The system state is augmented with an adaptive filter part containing process coefficients $\tilde{\boldsymbol{x}}^{p}_{k+1}$ regarding the shaping filter. This leads to the following system equations where the relationship between shaping filter and process coefficient is represented by the matrix $\boldsymbol{T}^{cp}_{k+1,k}$. The standard Kalman filter part remains the same (first row in extended transition matrix).

$$\begin{vmatrix} \tilde{\boldsymbol{x}}_{k+1} \\ \boldsymbol{\varepsilon}^{c}_{k+1} \\ \tilde{\boldsymbol{x}}^{p}_{k+1} \end{vmatrix} = \begin{vmatrix} \boldsymbol{T}_{k+1,k} & \boldsymbol{0} & \boldsymbol{0} \\ \boldsymbol{0} & \boldsymbol{T}^{c}_{k+1,k} & \boldsymbol{T}^{cp}_{k+1,k} \\ \boldsymbol{0} & \boldsymbol{0} & \boldsymbol{I}^{p} \end{vmatrix} \cdot \begin{vmatrix} \tilde{\boldsymbol{x}}_{k} \\ \boldsymbol{\varepsilon}^{c}_{k} \\ \tilde{\boldsymbol{x}}^{p}_{k} \end{vmatrix} + \begin{vmatrix} \boldsymbol{B}_{k+1,k} \\ \boldsymbol{0} \\ \boldsymbol{0} \end{vmatrix} \cdot \tilde{\boldsymbol{u}}_{k} + \begin{vmatrix} \boldsymbol{C}_{k+1,k} & \boldsymbol{0} & \boldsymbol{0} \\ \boldsymbol{0} & \boldsymbol{C}^{c}_{k+1,k} & \boldsymbol{C}^{cp}_{k+1,k} \\ \boldsymbol{0} & \boldsymbol{0} & \boldsymbol{I}^{p} \end{vmatrix} \cdot \begin{vmatrix} \boldsymbol{w}_{k} \\ \boldsymbol{w}^{c}_{k} \\ \boldsymbol{w}^{p}_{k} \end{vmatrix}. \tag{11}$$

As can be seen in the third row of the equation (11), the prediction of the process coefficient is modelled by a random walk process, excited by white noise.

The measurement equations have to be extended by zeros because the adaptive process coefficients are generally not observable

$$\boldsymbol{l}'_{k+1} = \begin{vmatrix} \boldsymbol{A}_{k+1} & \boldsymbol{A}^{c}_{k+1} & \boldsymbol{0} \end{vmatrix} \cdot \begin{vmatrix} \tilde{\boldsymbol{x}}_{k+1} \\ \boldsymbol{\varepsilon}^{c}_{k+1} \\ \tilde{\boldsymbol{x}}^{p}_{k+1} \end{vmatrix} + \boldsymbol{\varepsilon}_{k+1}. \tag{12}$$

4. Position Estimation

This chapter provides a short overview about the realisations of the two in chapter 3.1 and 3.2 described filter models. The base for the modifications shown trace back to the standard Kalman filter approach for kinematic positioning realised at IAGB, see [14], [15]. The trajectory is represented by a non-accelerated circular motion, the state quantities are position, orientation and velocity. Input quantities are orientation differences, distances and positions from differential GPS. For further information see [15], [16].

4.1. Model 1: Shaping Filter

The shaping filter approach contains the system states of the standard filter and is augmented by deviations along (l) and cross track (q) for consideration of the red noise process evaluated in chapter 2. The non-linear prediction of the system state is calculated

$$\begin{aligned}
\bar{y}_{k+1} &= \hat{y}_{k} + \cos\hat{\alpha}_{k} \cdot \frac{\hat{v}_{k}\ \Delta t}{\Delta\alpha_{k+1}}\ (1-\cos\Delta\alpha_{k+1}) + \sin\hat{\alpha}_{k} \cdot \frac{\hat{v}_{k}\ \Delta t}{\Delta\alpha_{k+1}}\ \sin\Delta\alpha_{k+1} \\
\bar{x}_{k+1} &= \hat{x}_{k} - \sin\hat{\alpha}_{k} \cdot \frac{\hat{v}_{k}\ \Delta t}{\Delta\alpha_{k+1}}\ (1-\cos\Delta\alpha_{k+1}) + \cos\hat{\alpha}_{k} \cdot \frac{\hat{v}_{k}\ \Delta t}{\Delta\alpha_{k+1}}\ \sin\Delta\alpha_{k+1} \\
\bar{\alpha}_{k+1} &= \hat{\alpha}_{k} + \Delta\alpha_{k+1} \\
\bar{v}_{k+1} &= \hat{v}_{k} \\
\bar{l}_{k+1} &= \hat{l}_{k} \cdot e^{-\beta^{2}\Delta t^{2}} \\
\bar{q}_{k+1} &= \hat{q}_{k} \cdot e^{-\beta^{2}\Delta t^{2}}
\end{aligned} \tag{13}$$

The measurement equations lead to the following innovations (compare equation (10))

$$\begin{aligned} d_{y'_{k+1}} &= y'_{k+1} - \left(\bar{y}_{k+1} - \bar{l}_{k+1} \cdot sin\,\bar{\alpha}_{k+1} - \bar{q}_{k+1} \cdot \cos\bar{\alpha}_{k+1}\right) \\ d_{x'_{k+1}} &= x'_{k+1} - \left(\bar{x}_{k+1} - \bar{l}_{k+1} \cdot \cos\bar{\alpha}_{k+1} + \bar{q}_{k+1} \cdot \sin\bar{\alpha}_{k+1}\right) \\ d_{s_{k+1}} &= s_{k+1} - \left(\bar{v}_{k+1} \cdot \Delta t\right) \\ d_{\Delta\alpha_{k+1}} &= \Delta\alpha_{k+1} - \left(\bar{\alpha}_{k+1} - \hat{\alpha}_k\right) \\ d_{s_{k+1}} &= s_{k+1} - \left(\bar{v}_{k+1} \cdot \Delta t\right) \end{aligned} \tag{14}$$

in which y'_{k+1}, x'_{k+1} indicate the DGPS positions including red measurement noise, two different sensors deliver distance information and one sensor orientation differences. The terms following the predicted y- respectively x-coordinates in the bracket expression model the influence of the deviations along and cross track.

4.2. Model 2: Adaptive Shaping Filter

In model 2 the attenuation factor β is implemented as process coefficient. Since it is modelled by a random walk process, the prediction equation is

$$\bar{\beta}_{k+1} = \hat{\beta}_k\,, \tag{15}$$

and the updated estimation is only depending on the stochastic model of the filter. Because the attenuation factor is now updated each epoch, the two additional shaping filter equations are

$$\begin{aligned} \bar{l}_{k+1} &= \hat{l}_k \cdot e^{-\hat{\beta}_k^2 \Delta t^2} \\ \bar{q}_{k+1} &= \hat{q}_k \cdot e^{-\hat{\beta}_k^2 \Delta t^2} \end{aligned} \tag{16}$$

in which the index k shows the variability of $\hat{\beta}_k$. It does not appear in the measurement equations (compare 3.2).

5. Evaluation

The potential for improvement of position estimation due to each filter modification presented has to be evaluated. This is done in two steps. First, variance-based sensitivity analysis with simulated data is applied to each filter approach to analyse the dependencies between input and output uncertainty. Second, some filter results of real data are exemplarily compared.

5.1. Variance-based Sensitivity Analysis

Variance-based sensitivity analysis is a useful tool to evaluate the uncertainty of output quantities of models in relation to the uncertainty of the respective input quantities. In addition it offers the possibility to determine not only qualitative but also quantitative correct results for models with arbitrary characteristics (e.g. linearity, additivity). Further information can be found in [17] and [18]. In [16] a representation of adaptation and interpretation of variance-based sensitivity analysis is given with respect to applications in kinematic positioning like focused herein.

Further on total order indices (compare [16], [19], [17]) are determined by the extended FAST method for the output quantities (system states) of each filter since the models are expected to be non-additive for the standard Kalman filter approach as stated in [19], [20]. The three filter approaches are abbreviated for simplicity: Kalman filter (KF), shaping filter (FF), adaptive shaping filter (AFF). The SimLab software, version 2.2, is used which is available at the website http://www.jrc.cec.eu.int/uasa/prj-sa-soft.asp. Two simulated scenarios are generated with sample sizes about 100.000.

The first scenario is a motion on a straight line for 10 epochs, where the initial orientation is $\alpha_0 = 50$ gon. In figure 2 the total order indices of the y-coordinate estimated by standard and the shaping filter are shown. Dependencies of the input variance to the output variance of the standard approach have been analysed in [20] and the analyses herein correspond in general. Main influence to the uncertainty of the y-coordinate is caused by its according measurement. The influence by the measured x-coordinate is also very high, this occurs due to the motion on a straight line with orientation of 50 gon. Since the total order indices are nearly the same for both filter approaches and this is also true for the x-coordinate, orientation and velocity, no statement about the mode of operation of the shaping filter can be made by this.

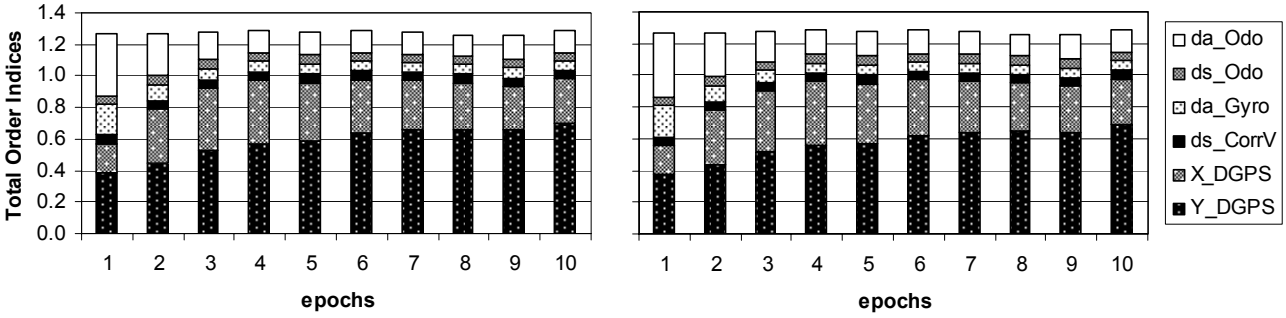

Figure 2: Total Order Indices of y-coordinate, KF (left) and FF (right), straight line, $\alpha_0 = 50$ gon

The standard deviations of the system states are computed by uncertainty analysis. In figure 3 the standard deviations of the y- and x-coordinates of the standard and the shaping filter are presented. Standard deviations are increasing up to the fourth epoch, this shows the influence of the variances of the initial system states, which are high in respect to the estimated one. Here also no significant differences between the two filter approaches can be determined. Higher standard deviations would have been expected, but the deviations along and cross track have only low influence on the standard deviations of the positions estimated by the shaping filter as they are very small (centimetre level) and their standard deviations, too.

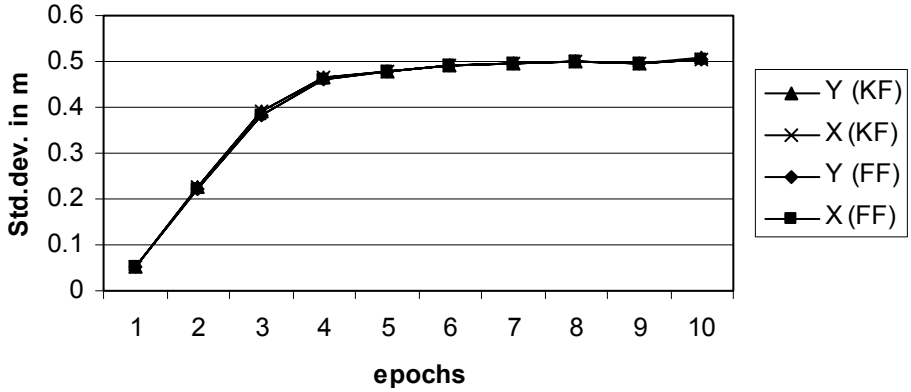

Figure 3: Standard deviations of the position estimations, KF and FF

To analyse the influence of the variance of the simulated measurements to the variance of the augmented system states in the shaping filter, sensitivity analysis is conducted for the deviations along and cross track. Their total order indices are shown in figure 4. Similar to the effect described above, both the variance of y- and x-coordinates from DGPS give the same influence to the variances along and cross track. The variance cross track is also influenced by the variance of the orientation differences. The main influence is caused by the differential odometer, because its variance is higher than the one of the gyro. Such effects have also been evaluated in [20].

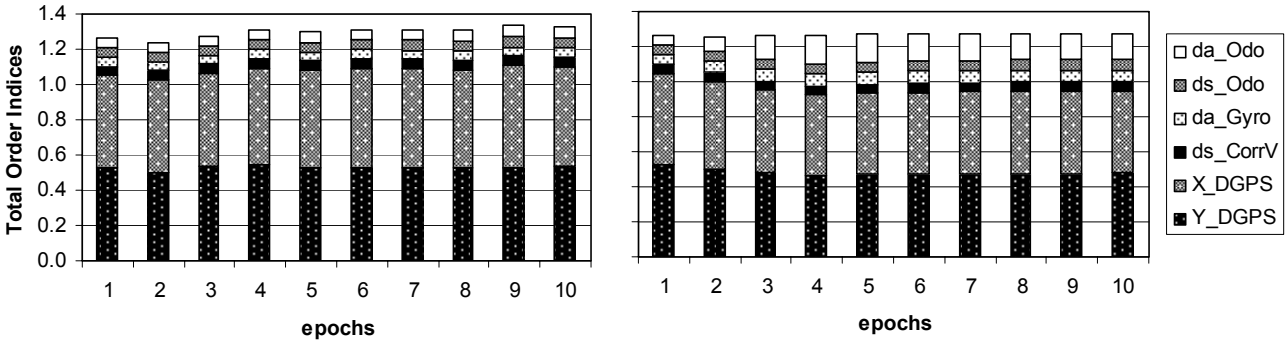

Figure 4: Total Order Indices along (left) and cross track (right), straight line, $\alpha_0 = 50$ gon

The second scenario evaluated is a motion on a straight line with initial orientation of $\alpha_0 = 0$ gon. Once again, in figure 5 the total order indices of the deviations along and cross track are shown. As expected, the main uncertainty along track results from uncertainty in the DGPS x-coordinate, while the main uncertainty cross track is given through the uncertainty of the DGPS y-coordinate and of the orientation differences by the differential odometer.

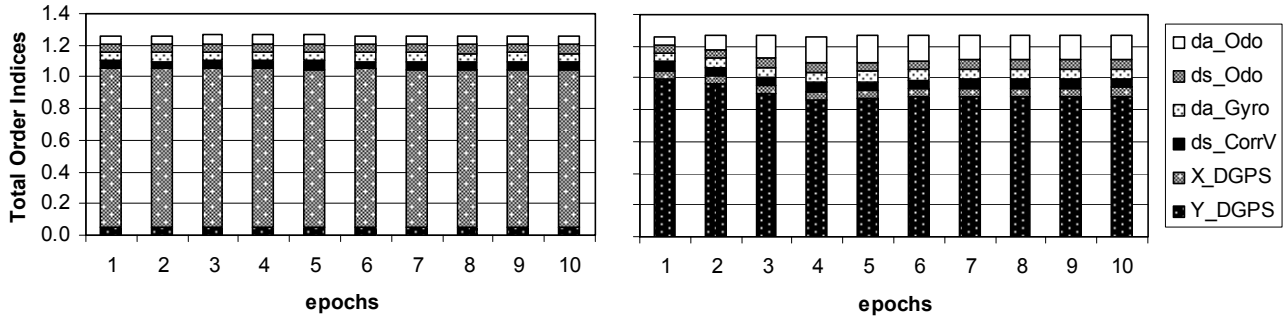

Figure 5: Total Order Indices along (left) and cross track (right), straight line, $\alpha_0 = 0$ gon

In the current stage of research, the sensitivity analysis of the adaptive shaping filter leads to the same results as the analysis of the shaping filter. The changes in the adaptive estimated attenuation factor are too small for an estimation within 10 epochs; so the respective total order indices are zero. The evaluation of more epochs is very time consuming because of the big sample sizes needed. Similar difficulties have already occurred while evaluating the shaping filter approach. The indirect influence of the deviations along and cross track to the position estimation can not be determined by the sensitivity analysis by now.

5.2. Real Data Analyses

The operation and the possible improvements by the modified filter approaches are now evaluated by means of real data from exemplarily chosen parts of the four test runs presented in chapter 2. Using the standard Kalman filter (KF), the shaping filter (FF) and the adaptive shaping filter (AFF) position estimation is carried out. The results estimated and the standard deviations of the system states are compared. This is exemplarily shown for test run 3 in this chapter.

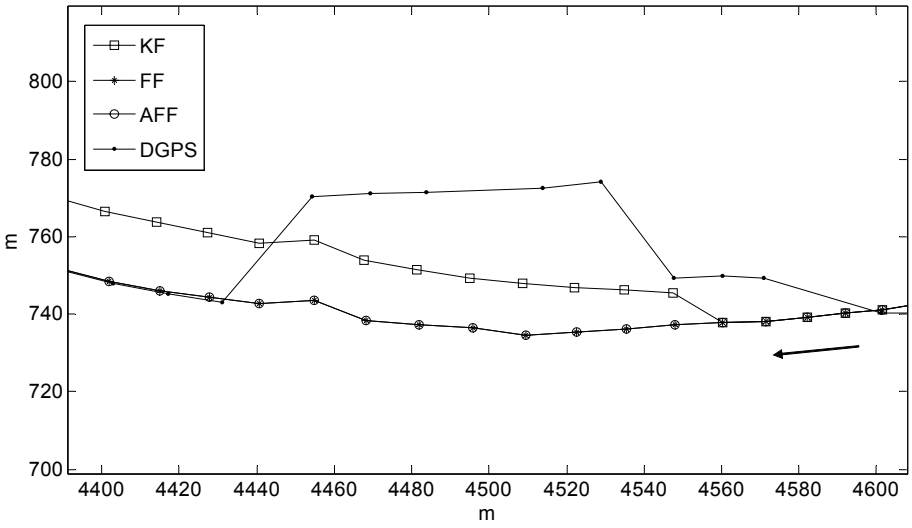

Figure 6: Results of filter estimations (KF, FF, AFF) using real data, example 1 in test run 3

In figure 6 a part of test run 3 is shown, where DGPS measurements of bad quality occur. For this case all three filter approaches described before are realised. Here the standard Kalman filter falsely forces the position estimation to the DGPS position. The shaping respectively adaptive shaping filter detects the bad DGPS quality and position estimation is improved by reducing the weight for the DGPS positions. This indicates a better quality of the filter tests due to the augmented modelling.

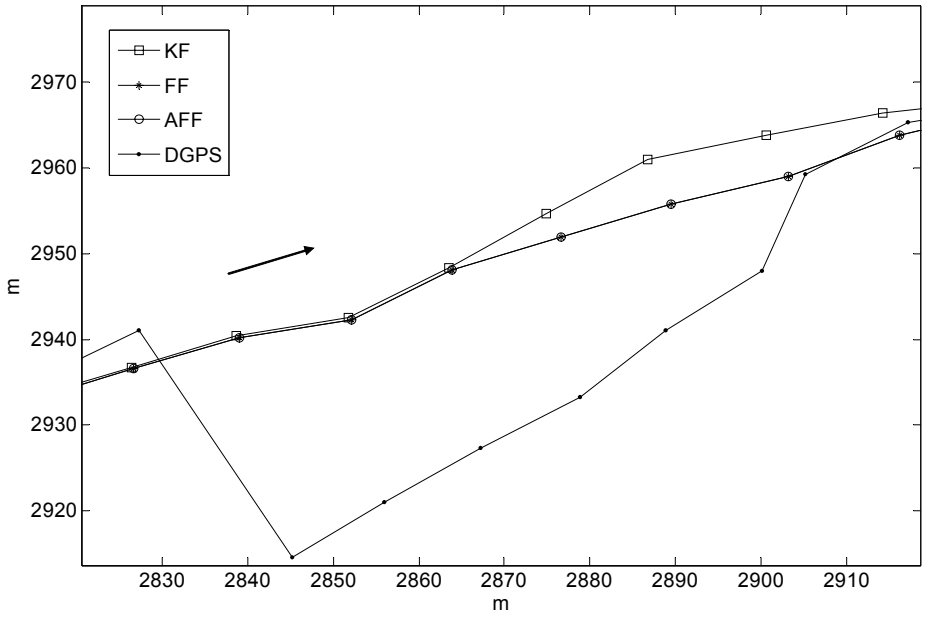

Figure 7: Results of filter estimations (KF, FF, AFF) using real data, example 2 in test run 3

In figure 7 also differences in position estimation are shown. The positions estimated by the (adaptive) shaping filter seem to be a bit smoother than the standard Kalman filter estimation. Both scenarios presented here are useful to evaluate possible improvements by modified filter approaches. Approx. 5 % of test run 3 the filter estimation differs for at least one approach. Methods to quantify these differences will be developed.

	KF	FF	AFF
s_Y **in m**	0.58	0.63	0.63
s_X **in m**	0.55	0.59	0.60
s_{alpha} **in gon**	2.37	2.35	2.35
s_v **in m/s**	0.10	0.10	0.10
s_l **in m**	n/a	0.25	0.25
s_q **in m**	n/a	0.24	0.24
s_{beta} **in 1/s**	n/a	n/a	0.0012

Table 3: Standard deviations of the three filter approaches for test run 3

In table 3 the standard deviations for each filter approach are tabulated. Summarised it can be stated, that the shaping filter approach actually results in slightly higher and therefore more realistic standard deviations for the position estimation. The standard deviation of the other output quantities remain unchanged. The adaptive shaping filter produces nearly the same results. In comparison the standard deviations of the position estimations correspond with those from simulated data, especially for the Kalman filter approach. The standard deviations of the deviations along and cross track is much higher than in the simulated case. This leads to the higher standard deviation for position estimation in the shaping filter. For this reason the importance is indicated to estimate more epochs also in case of simulated data.

6. Conclusion and Future Outlook

The augmentation of the standard Kalman filter to a shaping respectively adaptive shaping filter has been successfully realised. Further work has to be done for evaluation of the achievable improvements. The sensitivity analysis as presented here indicates no difference in position estimation between the three filter approaches. The expected influence of the DGPS measurements to the deviations along and cross track can be shown. By now the influence of the deviations along and cross track to the position estimation can not be evaluated. Two reasons are conceivable: On the one hand, the simulated input quantities for the DGPS measurements are generated with normal distribution and white measurement noise since no consideration of time-related correlation is possible for the extended FAST in SimLab. This leads to a very small estimation of the deviations along and cross track and their respective standard deviations, which are higher in real data estimation. On the other hand, probably another method for sensitivity analysis has to be applied since the deviations along and cross track act like input quantities in relation to the DGPS measurements. This is not explicitly considered yet. These investigations have to be transferred to the evaluation of the adaptive estimated attenuation factor. Further methods to prove the determination of this process coefficient within the given model setup have to be applied. Nevertheless, improvements of position estimation by shaping filter augmentation are shown in real data, indicating the importance of the augmentation implemented. The improvements have to be quantified appropriate.

References:

[1] Kalman, R. E.: A New Approach to Linear Filtering and Prediction Problems. Transactions of the ASME – Journal of Basic Engineering, Vol. 82, Series D, p. 35-45, 1960.

[2] Gelb, A.: Applied Optimal Estimation. The M.I.T. Press, Massachusetts Institute of Technology. Cambridge, Massachusetts and London, England, 1974.

[3] Heunecke, O.: Zur Identifikation und Verifikation von Deformationsprozessen mittels adaptiver KALMAN-Filterung (Hannoversches Filter). Wissenschaftliche Arbeiten der Fachrichtung Vermessungswesen der Universität Hannover, Heft 208, 1995.

[4] Huep, W.: Zur Positionsschätzung im gestörten KALMAN-Filter am Beispiel eines manövrierenden Wasserfahrzeuges. Wissenschaftliche Arbeiten der Fachrichtung Vermessungswesen der Universität Hannover, Nr. 143, 1986.

[5] Chui, C. K., Chen, G.: Kalman Filtering with Real-Time Applications. Springer-Verlag, Berlin Heidelberg, 1999.

[6] Schwieger, V.: Ein Elementarfehlermodell für GPS-Überwachungsmessungen – Konstruktion und Bedeutung interepochaler Korrelationen. Wissenschaftliche Arbeiten der Fachrichtung Vermessungswesen der Universität Hannover, Nr. 231, 1999.

[7] Howind, J.: Analyse des stochastischen Modells von GPS-Trägerphasenbeobachtungen. Deutsche Geodätische Kommission, Reihe C, Nr. 584, 2005.

[8] Hofmann-Wellenhof, B., Lichtenegger, H., Collins J.: GPS – Theory and Practice. Springer-Verlag, Wien New York, 1994.

[9] El-Rabbany, A. E-S.: The Effect of Physical Correlations on the Ambiguity Resolution and Accuracy Estimation in GPS Differential Positioning. Ph.D. dissertation, Department of Geodesy and Geomatics Engineering Technical Report No. 170, University of New Brunswick, Fredericton, Canada, 161 pp., 1994.

[10] El-Rabbany, A. E-S., Kleusberg, A.: Effect of Temporal Physical Correlation on Accuracy in GPS Relative Positioning. Journal of Surveying Engineering, Vol. 129, No. 1, February 2003.

[11] Kuhlmann, H.: KALMAN-Filtering with Coloured Measurement Noise for Deformation Analysis, Proceedings, 11th FIG Symposium on Deformation Measurements, Santorini, Greece, 2003.

[12] Wells, D. E., Beck, N., Delikaraoglu, D., Kleusberg, A., Krakiwsky, E. J., Lachapelle, G., Langley, R. B., Nakiboglu, M., Schwarz, K. P., Tranquilla, J. M., Vanicek, P.: Guide to GPS Positioning. Canadian GPS Associates, Fredericton, N. B., Canada, 1986.

[13] Taubenheim, J.: Statistische Auswertung geophysikalischer und meteorologischer Daten. Akademische Verlagsgesellschaft Geest und Portig K.-G., Leipzig, 1969.

[14] Eichhorn, A.: Ein Beitrag zur parametrischen Identifikation von dynamischen Strukturmodellen mit Methoden der adaptiven Kalman Filterung. DGK, Reihe C, Heft 585, München, 2005.

[15] Ramm, K., Schwieger, V.: Multisensorortung für Kraftfahrzeuge. In: Schwieger, V., Foppe, K. (Ed., 2004): Kinematischen Messmethoden – Vermessung in Bewegung, DVW Schriftenreihe, Band 45, Wißner Verlag, Augsburg, 2004.

[16] Schwieger, V.: Sensitivity Analysis as a General Tool for Model Optimisation – Examples for Trajectory Estimation. Proceedings on 3rd IAG Symposium on Structural Engineering, Baden, Austria, 22nd – 24th May 2006.

[17] Saltelli, A., Chan, K., Scott, E.M. (Ed.): Sensitivity Analysis. John Wiley and Sons, Chichester, 2000.

[18] Saltelli, A., Tarantola, S., Campolongo, F., Ratto, M.: Sensitivity Analysis in Practise. John Wiley and Sons, Chichester, 2004.

[19] Schwieger, V.: Nicht-lineare Sensitivitätsanalyse, gezeigt an Beispielen zu bewegten Objekten. Deutsche Geodätische Kommission, Reihe C, Nr. 531, 2005.
[20] Wilhelm, D.: Ein Beitrag zur Validierung zweier Modellierungsansätze für bewegte Fahrzeuge unter Nutzung der varianz-basierten Sensitivitätsanalyse. Study Thesis at IAGB, Universität Stuttgart, 2005 (unpublished).
[21] Schwieger, V., Schollmeyer, R., Ramm, K.: Integrated Positioning by MOPSY. Proceedings on 5th European Congress and Exhibition on Intelligent Transport Systems and Services, Hannover, 01.-03.06. 2005.